Journal of Medicinal Chemistry Article

J. Med. Chem. 2011, 54, 457–471 457
DOI: 10.1021/jm100843z

Pyrimidine Derivatives as Potent and Selective A_3 Adenosine Receptor Antagonists

Vicente Yaziji,[†,‡] David Rodríguez,[§] Hugo Gutiérrez-de-Terán,*[,§] Alberto Coelho,[†,‡] Olga Caamaño,[#] Xerardo García-Mera,[#] José Brea,[∥] María Isabel Loza,*[,∥] María Isabel Cadavid,[∥] and Eddy Sotelo*[,†,‡,#]

[†]*Combinatorial Chemistry Unit (COMBIOMED), Institute of Industrial Pharmacy,* [‡]*Center for Research in Biological Chemistry and Molecular Materials, University of Santiago de Compostela,* [§]*Public Galician Foundation of Genomic Medicine, Santiago de Compostela University Hospital (CHUS), 15706, Santiago de Compostela, Spain,* [#]*Department of Organic Chemistry, and* [∥]*Department of Pharmacology, Faculty of Pharmacy, University of Santiago de Compostela, Santiago de Compostela, 15782, Spain*

Received June 11, 2010

Two regioisomeric series of diaryl 2- or 4-amidopyrimidines have been synthesized and their adenosine receptor affinities were determined in radioligand binding assays at the four human adenosine receptors (hARs). Some of the ligands prepared herein exhibit remarkable affinities ($K_i < 10$ nm) and, most noticeably, the absence of activity at the A_1, A_{2A}, and A_{2B} receptors. The structural determinants that support the affinity and selectivity profiles of the series were highlighted through an integrated computational approach, combining a 3D-QSAR model built on the second generation of GRid INdependent Descriptors (GRIND2) with a novel homology model of the hA_3 receptor. The robustness of the computational model was subsequently evaluated by the design of new derivatives exploring the alkyl substituent of the exocyclic amide group. The synthesis and evaluation of the novel compounds validated the predictive power of the model, exhibiting excellent agreement between predicted and experimental activities.

Introduction

The ubiquitous nucleoside adenosine is essential for the proper functioning of every cell in mammalian species. Adenosine is directly linked to energy metabolism through ATP, ADP, and AMP, while at the extracellular level it regulates a wide range of biological functions through activation of specific receptors (adenosine receptors, ARs),[1−3] which are classified as A_1, A_{2A}, A_{2B}, and A_3[4] and belong to the superfamily of the G-protein coupled receptors (GPCRs[a]). The improved understanding of the physiology, pharmacology, structure, and molecular biology of adenosine and its receptors has provided solid foundations that support the potential the development of conceptually unexplored therapeutic strategies to address serious unmet medical needs. The advances in the medicinal chemistry of this emerging family of therapeutics have been reviewed recently.[5−7]

The A_3AR subtype is the most recently characterized member of the family.[8] Activation[9,10] of this subtype has been shown to inhibit adenylate cyclase, to increase phosphatidylinositol-specific phospholipase C and D activity, to elevate intracellular Ca^{2+} and IP_3 levels, and to enhance the release of inflammatory and allergic mediators from mast cells. The therapeutic applications derived from the modulation of this receptor subtype have been reviewed recently.[11−18] In particular, it is becoming increasingly apparent that antagonists of A_3AR might be therapeutically useful for the acute treatment of stroke and glaucoma,[19] inflammation,[20−22] and in the development of cerebroprotective,[23,24] antiasthmatic and antiallergic drugs.[25,26] Furthermore, recent evidence[27−31] of high levels of expression of A_3ARs in several cell lines has suggested potential applications for A_3AR antagonists in cancer chemotherapy.

The putative applications of these compounds as drugs, as well as the growing demand for pharmacological tools to study the human A_3AR roles, has made the identification of potent and selective small molecule antagonists of this receptor subtype a topic of great interest.[11−18] The search for A_3AR antagonists began with the observation that xanthines — a successful structural motif in the search for antagonists for the other ARs subtypes — exhibit low binding affinities for the A_3 receptor subtype. The pursuit of A_3AR antagonists therefore focused on the exploration of structurally diverse heterocyclic libraries. Nowadays, the best known class of A_3AR ligands (Figure 1) includes highly diverse families of tri- and bicyclic heteroaromatic scaffolds and, to a lesser extent, mono-heterocyclic systems. Whereas the systematic structural elaboration of these prototypes has provided derivatives possessing good affinity,[11−18] the selectivity issue and the relatively poor bioavailability profiles of drug candidates have remained elusive until recently.[5−7]

The pyrimidine core, being part of the heterocyclic moiety of the endogenous ligand of these receptors (adenosine), is a recurrent substructural motif within bi- and tricyclic ARs antagonists.[5−7] The well-documented contributions of this chemotype to the field notwithstanding, relatively few papers

*To whom correspondence should be addressed. (H.G.) tel.: ++34-881813873, e-mail: hugo.teran@usc.es. (M.I.L.) tel.: ++34-881815005, e-mail: mabel.loza@usc.es. (E.S.) tel.: ++34-881815221, Fax.: ++34-981-528093, e-mail: eddy.sotelo@usc.es.

[a] Abbreviations: hARs, human adenosine receptors; ADP, adenosine diphosphate; ATP, adenosine-5′-triphosphate; AMP, adenosine monophosphate; GPCRs, G-protein coupled receptors; 3D-QSAR, three-dimensional quantitative structure−activity relationships, GRIND2, GRid INdependent Descriptors; IP_3, inositol trisphosphate; CHO cells, Chinese hamster ovary cells; CLACC, consistency large auto and cross correlation; MIF, molecular interaction fields; PDB, Protein Data Bank; LOO, leave-one out; rmsd, root mean square deviation.

Published on Web 12/27/2010

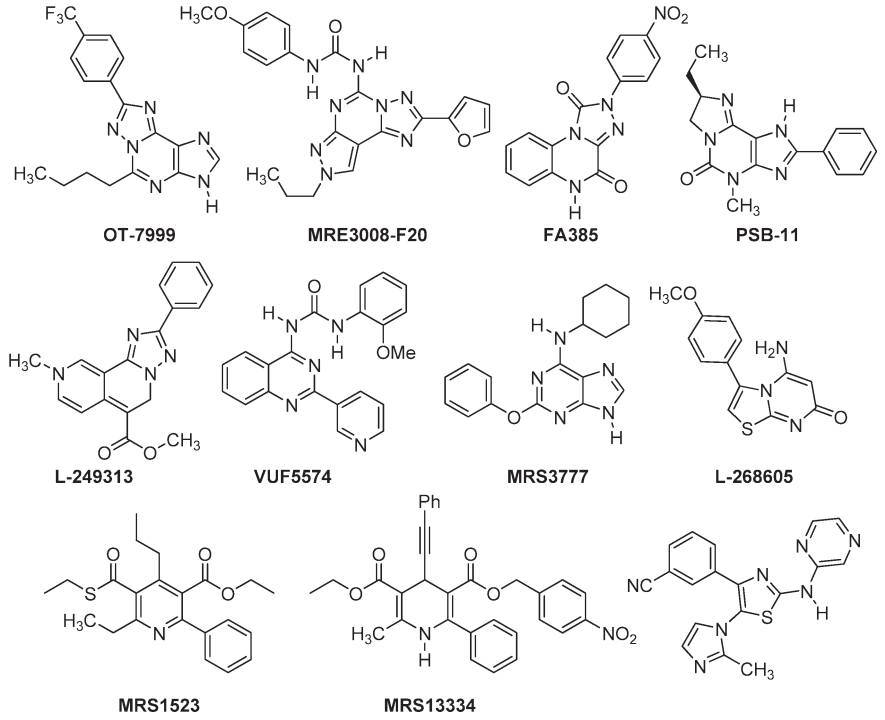

Figure 1. Structures of representative selective A_3 adenosine receptor antagonists.

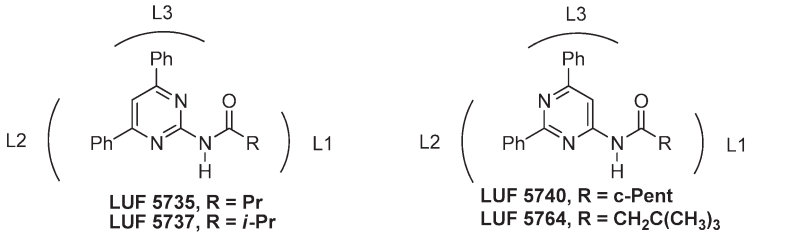

Code	hA_1[¥]	hA_{2A}[¥]	hA_{2B}[¥]	hA_3[¥]	Code	hA_1[¥]	hA_{2A}[¥]	hA_{2B}[¥]	hA_3[¥]
LUF5735	3.70	7%	54%	38%	**LUF5740**	2.14	196.00	52%	170.00
LUF5737	8.87	44%	79%	45%	**LUF5764**	8.75	32%	4%	39%

[¥] Adenosine binding data is expressed as K_i (nM) or as % of displacement at 1 μM.[39]

Figure 2. Structures and biological data for representative diphenyl 2- or 4-amidopyrimidines as selective A_1 adenosine receptor antagonists. The substitutions further explored in the present report follow those established in the early A_1AR model,[39] labeled as L1, L2, and L3, indicating the lipophilic pockets in the receptor. Note that there is no substitutuent in L1 in the series of aminopyrimidines and that L2 = L3 for all compounds described herein.

have concerned focused programs based on this scaffold,[32−36] or its biososters (e.g., triazines).[37] Two recent publications have covered (1) a molecular simplification study from triazoloquinoxalines to pyrimidines[38] and (2) the elaboration of a pharmacophoric model for A_1 adenosine receptors, based on structurally simple regioisomeric diarylpyrimidine scaffolds (Figure 2).[39] The latter work not only enabled the identification of potent and selective A_1AR antagonists derived from either the 4,6-diphenyl-2-amidopyrimidine or 2,6-diphenyl-4-amidopyrimidine templates (Figure 2) but also provided a valuable structural model that could be exploited for the design of new series of compounds.

In light of these precedents, and particularly residual activity toward the hA_3AR subtype observed for some previously reported compounds (Figure 2),[39] it was envisioned that the structural redecoration of the aryl fragments on the amidopyrimidine templates would modify the adenosine receptor selectivity profile and provide new selective A_3AR antagonists. We therefore focused on the exploration of diverse aryl moieties on the heterocyclic scaffold, with particular attention paid to structural elements that had been previously identified as contributors in the molecular recognition of the A_3AR subtype (e.g., 4-methoxyphenyl group).[40−43] From methodological and practical points of view, it was decided first to explore the synthesis and screening of libraries incorporating identical aryl groups at positions 4,6 and 2,6, as a proof of concept. Thereafter, depending on the results of this first series (reported in the current manuscript) the synthesis of nonidentical series will be performed. The design of the new chemical entities was assisted, and interpreted, by developing an integrated molecular modeling approach that combined ligand docking and 3D quantitative-structure activity (3D-QSAR) studies. Although limitations in the homology modeling of ARs in the design of new ligands have recently been recognized,[44−46] the recent release of the crystal structure of human A_{2A}AR in complex with the potent inhibitor 4-(2-[7-amino-2-(2-furyl)[1,2,4]triazolo[2,3-*a*][1,3,5]triazin-5-ylamino]-ethyl)phenol (ZM241385)[47] has been a breakthrough in this

Scheme 1[a]

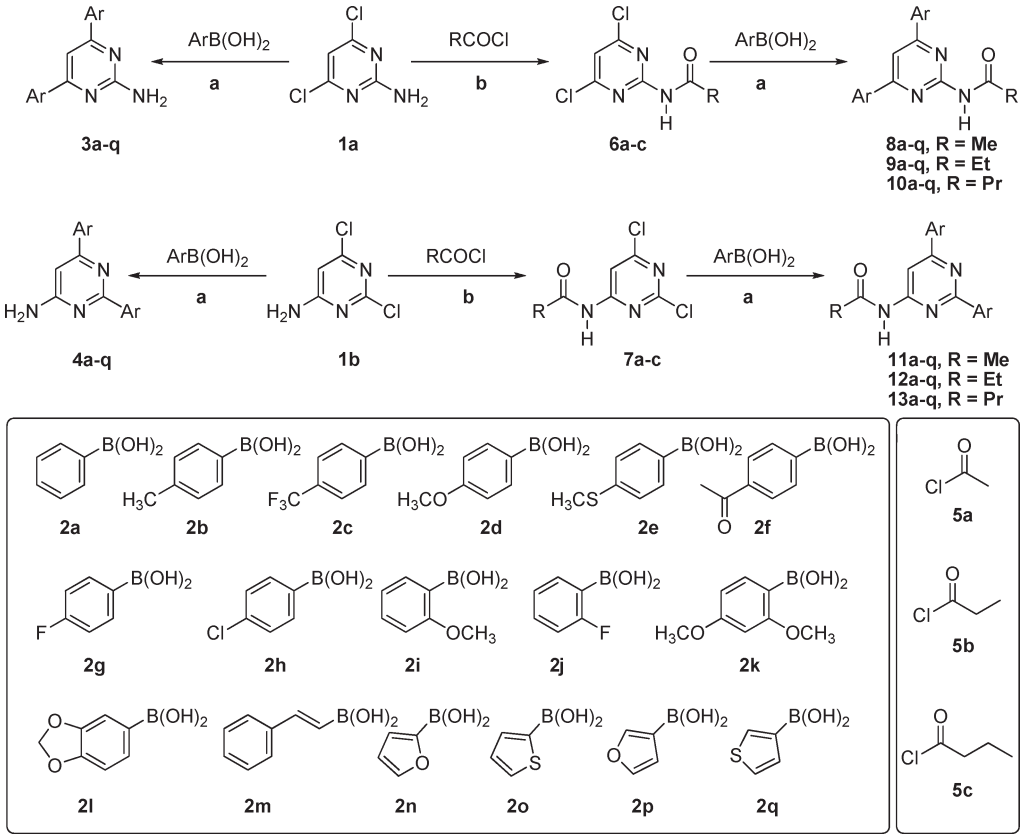

[a] Reagents: (a) $Pd[(PPh)_3]_4$, DME/H_2O, Na_2CO_3, (b) THF, TEA.

area, as occurred earlier with the release of the structure of the hβ_2 adrenergic receptor.[49] In fact, the most recent models of the A_3AR have already taken advantage of this crystal structure in the description of receptor−antagonist recognition.[48] On the other hand, structure-based approaches have frequently been combined in G protein-coupled receptor (GPCR) research with ligand-based techniques, such as pharmacophore models[39] or 3D-QSAR studies.[46] In the present work, a new A_3AR model, derived from the recent crystal structure of $A_{2A}AR$, is reported and used as a basis for the automated docking of the series reported here. In a first iteration, an initial batch of compounds was synthesized, tested, and computationally investigated for the binding mode of the series, which guided the design of the rest of the compounds series. Once the experimental affinities were available for the compounds here reported, the new ligands were computationally described and their structure−affinity was modeled by using the most recent version of the GRid INdependent Descriptors (GRIND-2),[50,51] thus providing a rational interpretation of the structure−activity and structure−selectivity relationships. To further challenge the computational model in terms of robustness and predictive capability, it was used for the design of novel compounds bearing new alkyl substitutions on the L1 site (see Figure 2). The synthesis and evaluation of the novel compounds validated the predictive power of the model, exhibiting excellent agreement between predicted and experimental activities.

Chemistry

Given that the feasibility of the proposed aim is heavily reliant on the exhaustive exploration of diverse (hetero)aryl residues on the functionalized pyrimidine templates, a short and divergent synthetic strategy was optimized.[52] The synthetic pathway developed to access the designed regioisomeric libraries is presented in Scheme 1, and this relied on the commercial availability of the 2- or 4-aminodichloropyrimidines **1a**−**b** as precursors. Application of the standard conditions of the highly reliable and well-established Suzuki−Miyaura cross-coupling reaction to a collection of commercially available boronic acids (**2a**−**q**), which representatively cover both the aryl and heteroaryl series (Scheme 1), enabled the rapid decoration of the heterocyclic core at positions 2,4- or 4,6- to afford diarylpyrimidinamines **3a**−**q** and **4a**−**q**, which can be considered bioisosteres of previously described 2-amino-4,6-diaryltriazines.[37] Derivatization of the amine function in the heterocyclic precursors **1a**−**b** by treatment with acid chlorides **5a**−**c** and subsequent palladium-catalyzed (hetero)arylation afforded two regiosomeric series of di(hetero)aryl 2- or 4-amidopyrimidines (**8**−**13**).

In an attempt to validate the robustness and predictive capability of the herein developed computational model some computer-generated new ligands, designed to evaluate the tolerance of A_3AR to the introduction of bulky alkyl residues in the amide moiety (L1) of the pyrimidin-4-amine series, were prepared. Treatment of two representative amines, incorporating binding residues that conferred high A_3 AR affinity (**4d** and **4k**), with three additional acid chlorides (Scheme 2) afforded the new structures **14a**−**f**.

The synthetic program provided a focused library of 142 members, which in turn can be subdivided into two regioisomeric sublibraries [34 amines (**3**−**4**) and 108 amides (**8**−**14**)] that were structurally characterized. A detailed account of the experimental procedures and the complete description of the

Scheme 2[a]

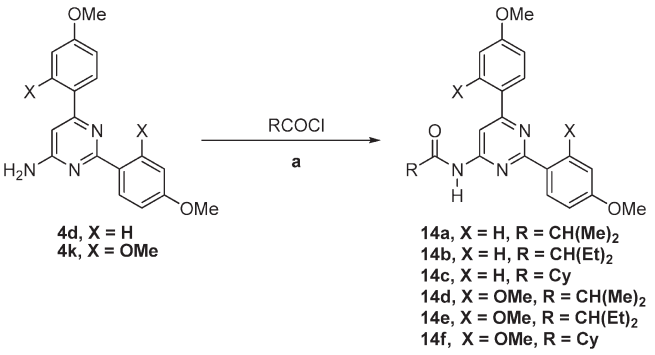

[a] Reagents: (a) THF, TEA.

analytical and spectroscopic data for all compounds are available in the Supporting Information.

Biological Evaluation

The affinities of the obtained compounds at the four human adenosine receptor subtypes were determined in vitro using radioligand binding assays according to experimental protocols described elsewhere.[53] Human adenosine receptors expressed in transfected CHO (A_1AR), HeLa (A_{2A}AR and A_3AR), and HEK-293 (A_{2B}AR) cells were employed. (^{3}H)-1,3-Dipropyl-8-cyclopentylxanthine ([^{3}H]DPCPX) for A_1AR and A_{2B}AR, [^{3}H]4-(2-[7-amino-2-(2-furyl)[1,2,4]triazolo[2,3-*a*][1,3,5]triazin-5-ylamino]ethyl)phenol for A_{2A}AR, and [^{3}H]NECA for A_3AR were employed as radioligands in binding assays. The biological data (Tables 1−3) are expressed as $K_i \pm$ SEM (nM, $n = 3$) or percentage of inhibition of specific binding at 0.1 μM (n = 2, average) for those compounds that did not fully displace radioligand binding.

Functional Assay at Adenosine A_3 Receptors

Some representative ligands that show affinity toward the hA_3AR subtype were also studied through cAMP experiments (see Figure 3 and Table 3). The functional evaluation was carried out with intact cells expressing the hA_3AR. The inhibition of forskolin-stimulated cAMP production by the receptor agonist was used as a read-out. Concentration−response curves of two representative compounds (compounds **11d** and **12d**) over 0.1 μM NECA-induced A_3AR activation are shown in Figure 3. cAMP formation was measured by enzyme immunoassay (GE Healthcare). Antagonistic potency, measured as K_B, was calculated from the formula: $K_B = (IC_{50})/((2 + ([A]/[A_{50}]^n)^{1/n} - 1)$, where IC_{50} is the concentration of the antagonist that inhibits the agonist stimulation by 50%, [A] is the concentration of the agonist in the assay, [A_{50}] is the concentration of the agonist that elicits the half-maximum response, and n is the slope of the concentration response curve.[54]

All these derivatives fully reverted the A_3AR-elicited inhibition of cAMP accumulation, unequivocally validating the antagonistic behavior of these compounds at the human A_3 AR. Moreover, a comparative analysis of the K_B values for these compounds (Table 3) during the cAMP experiments revealed a clear correspondence with the affinity values determined during the binding experiments (K_i in Table 4).

Structure−Activity Relationship and Molecular Modeling

Affinities in radioligand binding assays at the four human adenosine receptors (A_1, A_{2A}, A_{2B}, and A_3) are reported for the 4,6-diaryl-2-amidopyrimidines (**8a−q−10a−q**, Table 1) and the 2,6-diaryl-4-amidopyrimidines (**11a−q−13a−q**, Table 2), as well as for the isomeric amine series (**3a−q** and **4a−q**, see Supporting Information). Examination of the binding data indicates that new potent and highly selective ligands for the A_3 receptor subtype have been identified (Table 2, compounds **11b**, **11d**, **12d**, **13d**, **11f**, **12h**, **11j**, **11k**, **12k**, **13k**, **11m**). These results validate the initial hypothesis that the appropriate decoration of the heterocyclic scaffold with previously unexplored diversities would lead to remarkable modifications in the pharmacological activity in comparison to the published results for analogous compounds. Moreover, the documented data exemplify how the structural manipulation of these privileged scaffolds is able to modify the biological profile, not only at the quantitative (affinity) level but also at the qualitative (selectivity) level.

Bearing in mind the considerable number of compounds tested, and for the sake of brevity and clarity, the analysis and interpretation of the data will be carried out at two levels. On the one hand, the most prominent features of the structure−activity (SAR) and structure−selectivity (SSR) relationships for both series will be discussed qualitatively. On the other hand, a more in-depth and quantitative structure−activity relationship can be obtained on the basis of an integrated molecular modeling study. Such an analysis was performed on the set of 64 compounds with experimental K_i values in the A_3 receptor, and this represents a novel approach based on the combination of molecular docking on a homology model for the A_3AR and a 3D-QSAR study.

It can be observed from the biological data the amine series (**3a−q** and **4a−q**) did not exhibit attractive pharmacological profiles at any of the ARs (see Supporting Information). The moderate affinity toward the A_1 receptor subtype elicited by the parent compounds of the regioisomeric series (Ar = Ph, compounds **3a** and **4a**) was generally extinguished by the introduction of groups at the phenyl rings or their replacement by diverse heterocyclic cores. The generally disappointing binding data are common to both regioisomeric amine subsets (**3** and **4**). The most remarkable derivative within the series (**4l**) combines a potent A_1AR antagonistic effect (K_i = 7.99 nM) and a satisfactory selectivity (> 30) versus the human A_3AR subtype.

Inspection of the pharmacological data obtained for the most populated set of compounds prepared in this work (i.e., the diaryl 2- or 4-amidopyrimidines **8a−q−13a−q**, Tables 1 and 2) confirms that the systematic modification of the structural prototypes produced a significant, but differentiated, variation in their biological behavior. A comparative analysis of these data highlights the different activity profiles elicited for the two regioisomeric series toward ARs (Tables 1 and 2). Thus, compounds that incorporate the amide moiety at position 4 of the heterocyclic core afforded the most interesting derivatives identified during this study, while their regioisomeric congeners gave a somewhat poor activity profile. Within the 2-amidopyrimidine series only those ligands bearing tolyl groups at positions 4 and 6 of the heterocyclic core (compounds **8b**, **9b**, and **10b**) and the *N*-[2,6-di(benzo-[d][1,3]dioxol-5-yl)pyrimidin-4-yl]acetamide (**8l**) elicited moderate A_3AR affinity (Table 1).

In clear contrast to previously discussed results for the amines (**3** and **4**) and 4,6-diaryl-2-amidopyrimidines (**8−10**), the biological data obtained for the 2,6-diaryl-4-amidopyrimidine subset (Table 2, compounds **11−13**) unequivocally show the determinant influence that the varied structural

Table 1. Structure and Affinity Binding Data for the 4,6-Diaryl-2-amidopyrimidines **8**, **9**, and **10** at the Human Adenosine Receptors

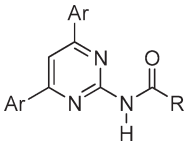

			K_i (nM) or % at 0.1 μM			
comp	Ar	R	hA_1[a]	hA_{2A}[b]	hA_{2B}[c]	hA_3[d]
8a	Ph	Me	17%	11%	6%	13%
9a		Et	31.3 ± 2.1	554 ± 32	42.5 ± 3.4	531 ± 31
10a		Pr	10.3 ± 1.9	3%	14%	17%
8b	4-Me-Ph	Me	3%	6%	3%	47.3 ± 4.7
9b		Et	1%	1%	3%	157 ± 22
10b		Pr	3760 ± 225	2%	10%	131 ± 19
8c	4-CF_3−Ph	Me	2%	1%	2%	10%
9c		Et	2%	12%	9%	2%
10c		Pr	1%	2%	13%	2%
8d	4-MeO-Ph	Me	1%	7%	1%	20%
9d		Et	2%	1%	8%	13%
10d		Pr	2%	24%	9%	15%
8e	4-MeS-Ph	Me	1%	1%	2%	14%
9e		Et	505 ± 36	183 ± 16	374 ± 22	4435 ± 85
10e		Pr	3%	7%	2%	3%
8f	4-MeCO-Ph	Me	7%	8%	14%	2%
9f		Et	1%	12%	1%	17%
10f		Pr	7%	14%	2%	22%
8g	4-F-Ph	Me	2%	2%	1%	8%
9g		Et	14%	3%	1%	22%
10g		Pr	18%	5%	2%	27%
8h	4-Cl-Ph	Me	2%	2%	1%	1%
9h		Et	1%	11%	2%	14%
10h		Pr	1%	3%	1%	17%
8i	2-F-Ph	Me	8%	12%	10%	15%
9i		Et	48.2 ± 4.6	424 ± 38	307 ± 19	279 ± 24
10i		Pr	23.5 ± 1.8	647 ± 101	6%	15%
8j	2-MeO-Ph	Me	4%	10%	1%	2%
9j		Et	21%	13%	2%	22%
10j		Pr	13%	11%	1%	18%
8k	2,4-MeO-Ph	Me	1%	2%	1%	9%
9k		Et	3%	14%	3%	17%
10k		Pr	14%	16%	15%	1%
8l	3,4- (CH_2−O_2)-Ph	Me	1%	15%	1%	101 ± 7
9l		Et	535 ± 37	16%	1%	127 ± 4
10l		Pr	678 ± 42	8%	1%	751 ± 18
8m	Ph−CH=CH-	Me	1%	15%	1%	4%
9m		Et	1%	1%	1%	142 ± 9
10m		Pr	1%	3%	2%	12%
8n	2-furan	Me	1%	19%	11%	9%
9n		Et	24%	15%	21%	1903 ± 116
10n		Pr	17%	23%	15%	1%
8o	2-thiophene	Me	2%	5%	3%	21%
9o		Et	24%	25%	2%	21%
10o		Pr	255 ± 31	201 ± 28	3%	24%
8p	3-furan	Me	1%	1%	1%	1%
9p		Et	3%	2%	11%	16%
10p		Pr	11%	17%	0%	21%
8q	3-thiophene	Me	2%	2%	1%	1%
9q		Et	367 ± 25	1893 ± 174	3250 ± 261	1279 ± 215
10q		Pr	85.7 ± 5.2	4568 ± 251	12%	2%

[a] Displacement of specific [^{3}H]DPCPX binding in human CHO cells expressed as K_i ± SEM in nM (n = 3) or percentage displacement of specific binding at a concentration of 0.1 μM (n = 2). [b] Displacement of specific [^{3}H]4-(2-[7-amino-2-(2-furyl)[1,2,4]triazolo[2,3-*a*][1,3,5]triazin-5-ylamino]ethyl)phenol binding in human HeLa cells expressed as K_i ± SEM in nM (n = 3) or percentage displacement of specific binding at a concentration of 0.1 μM (n = 2). [c] Displacement of specific [^{3}H]DPCPX binding in human HEK-293 cells expressed as K_i ± SEM in nM (n = 3) or percentage displacement of specific binding at a concentration of 0.1 μM (n = 2). [d] Displacement of specific [^{3}H]NECA binding in human HeLa cells expressed as K_i ± SEM in nM (n = 3) or percentage displacement of specific binding at a concentration of 0.1 μM (n = 2).

parameters have on the antagonistic profile of these series. The exhaustive exploration of the scaffold enabled the identification of structurally simple derivatives that exhibit outstanding affinity and remarkable selectivity for the A_3AR

Table 2. Structure and Affinity Binding Data for the 2,6-Diaryl-4-amidopyrimidines **11**, **12**, and **13** at the Human Adenosine Receptors

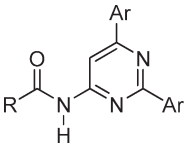

			K_i (nM) or % at 0.1 μM			
comp	Ar	R	hA_1[a]	hA_{2A}[b]	hA_{2B}[c]	hA_3[d]
11a	Ph	Me	31.2 ± 4.1	255.3 ± 13	19%	12.1 ± 1.3
12a		Et	22.3 ± 3.3	84.5 ± 5.7	76.6 ± 6.4	45.5 ± 7.4
13a		Pr	19.5 ± 3.2	103 ± 8	1%	171 ± 21
11b (ISVY133)	4-Me-Ph	Me	2%	8%	2%	4.4 ± 0.3
12b		Et	36.9 ± 4.1	1%	2%	18.3 ± 1.9
13b		Pr	16%	2%	3%	59.0 ± 2.3
11c	4-CF_3−Ph	Me	1%	1%	1%	126 ± 11
12c		Et	3%	17%	8%	12%
13c		Pr	3%	1%	6%	12%
11d (ISVY130)	4-MeO-Ph	Me	1%	10%	4%	3.6 ± 0.2
12d (ISVY074)		Et	8%	1%	3%	3.6 ± 0.40
13d (ISVY071)		Pr	8%	4%	1%	11.0 ± 1.3
11e	4-MeS-Ph	Me	1%	1%	2%	71.3 ± 3.5
12e		Et	1%	1%	3%	43.6 ± 1.7
13e		Pr	3%	2%	1%	12%
11f	4-MeCO-Ph	Me	10%	13%	16%	25.2 ± 0.7
12f		Et	1%	1%	2%	43.9 ± 2.4
13f		Pr	2%	1%	1%	133 ± 20
11g	4-F-Ph	Me	15%	1334 ± 110	1%	16.7 ± 1.4
12g		Et	83.9 ± 5.0	429 ± 18	1%	12.1 ± 0.6
13g		Pr	82.3 ± 3.4	1829 ± 47	2%	34.8 ± 3.1
11h	4-Cl-Ph	Me	1%	10%	1%	63.3 ± 8.2
12h		Et	16%	20%	3%	25.3 ± 0.5
13h		Pr	16%	21%	1%	103 ± 6
11i	2-F-Ph	Me	17%	73.8 ± 6.0	21%	18.1 ± 0.7
12i		Et	31.6 ± 4.1	103 ± 5	16%	160 ± 14
13i		Pr	18.7 ± 2.5	142 ± 7	9%	135 ± 11
11j	2-MeO-Ph	Me	1%	14%	1%	24.1 ± 1.3
12j		Et	113 ± 9	22%	7%	23.2 ± 0.8
13J		Pr	41.3 ± 2.6	14%	3%	110 ± 15
11k (ISVY167)	2,4-MeO-Ph	Me	1%	6%	2%	5.4 ± 0.1
12k (ISVY169)		Et	6%	14%	8%	11.3 ± 1.4
13k		Pr	18%	12%	14%	10.2 ± 1.1
11l	3,4- (CH_2−O_2)-Ph	Me	17.7 ± 3.1	3345 ± 127	2%	3.3 ± 0.3
12l		Et	5.28 ± 0.8	2541 ± 64	1668 ± 39	14.5 ± 1.2
13l		Pr	9.7 ± 1.4	22%	16%	59.0 ± 4.3
11m	Ph−CH=CH-	Me	1%	13%	1%	15.6 ± 2.1
12m		Et	17%	2%	2%	46.9 ± 5.4
13m		Pr	1%	1%	8%	25%
11n	2-furan	Me	40.7 ± 5.2	8.1 ± 1.2	12.0 ± 1.1	3.0 ± 0.4
12n		Et	15.5 ± 3.1	6.4 ± 0.7	20.5 ± 2.4	6.2 ± 0.7
13n		Pr	7.8 ± 0.9	5.7 ± 0.4	16.4 ± 0.7	9.9 ± 1.2
11o	2-thiophene	Me	19%	24.6 ± 2.6	23%	8.0 ± 0.4
12o		Et	32.9 ± 1.4	114 ± 7	17%	21.8 ± 2.2
13o		Pr	33.3 ± 3.2	153 ± 11	8%	23.0 ± 4.0
11p	3-furan	Me	1%	74.0 ± 3.2	302 ± 67	10.1 ± 0.9
12p		Et	132 ± 10	82.8 ± 6.0	49.0 ± 5.3	12.6 ± 1.1
13p		Pr	65.1 ± 4.0	544 ± 11	1%	3%
11q	3-thiophene	Me	13%	39.8 ± 4.4	16%	20.2 ± 3.2
12q		Et	39.4 ± 2.3	63.5 ± 4.1	164.7 ± 47	64.2 ± 5.6
13q		Pr	65.1 ± 4.7	23%	21%	11%

[a] Displacement of specific [^{3}H]DPCPX binding in human CHO cells expressed as K_i ± SEM in nM (n = 3) or percentage displacement of specific binding at a concentration of 0.1 μM (n = 2). [b] Displacement of specific [^{3}H]4-(2-[7-amino-2-(2-furyl)[1,2,4]triazolo[2,3-*a*][1,3,5]triazin-5-ylamino]ethyl)phenol binding in human HeLa cells expressed as K_i ± SEM in nM (n = 3) or percentage displacement of specific binding at a concentration of 0.1 μM (n = 2). [c] Displacement of specific [^{3}H]DPCPX binding in human HEK-293 cells expressed as K_i ± SEM in nM (n = 3) or percentage displacement of specific binding at a concentration of 0.1 μM (n = 2). [d] Displacement of specific [^{3}H]NECA binding in human HeLa cells expressed as K_i ± SEM in nM (n = 3) or percentage displacement of specific binding at a concentration of 0.1 μM (n = 2).

(see Table 2, compounds **11b**, **11d**, **12d**, **13d**, **11k**, **12k**, **13k**). A comparison of these data with the observed activity for the parent compounds of the series (Table 2, Ar = Ph, compounds **11a**, **12a**, **13a**, relatively A_1AR potent but somewhat

Table 3. Antagonistic Potency (Measured as K_B) at Human A_3 Receptors of Selected Compounds[a]

compound	K_B (nM)
12d	1.40 ± 0.09
13d	1.57 ± 0.13
11k	3.85 ± 0.41
11b	3.56 ± 0.23
12h	3.88 ± 1.17

[a] Values represent the mean ± SEM of two separate experiments.

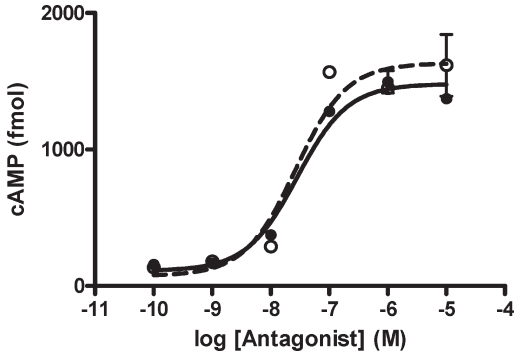

Figure 3. Effect of **11d** (○, dashed fitting) and **12d** (●, black fitting) on 0.1 μM NECA-induced cAMP decrease of 10 μM forskolin-stimulated human A_3 receptors. Points represent the mean ± SEM (vertical bars) of two separate experiments.

promiscuous AR ligands) allows the rapid evaluation of the effects caused by the structural modifications. In general, modification of the aromatic substitution pattern completely extinguished the affinity for the A_1AR, while conferring notable potency and selectivity toward the A_3AR subtype. Remarkably, such a subtle structural modification is able to produce a radical variation in the activity profile, being significant not only for a methoxy group at position 4 but also for the more highly diverse residues explored (e.g., methyl, thiomethyl, acetyl, fluoro and chloro). It is also remarkable that the vinyl analogues (Table 2, compounds **11m** and **12m**) of the parent compounds proved to be relatively potent and highly selective A_3 ligands, a finding that reaffirms how bulky substituents at sites L2/L3 favor selectivity toward hA_3AR. The consequences of introducing a group at position 2 of the phenyl ring was also briefly assessed (Table 2, compounds **11i**, **12i**, **13i**, **11j**, **12j**, and **13j**). As observed, the introduction of fluoro or methoxy groups at this position afforded relatively potent derivatives, albeit with markedly different selectivity profiles. Within this ligand subset only the 2-methoxyphenyl derivative of the 4-acetamide series (compound **11i**) elicited a satisfactory affinity/selectivity profile. Conversely, the simultaneous introduction of methoxy groups at positions 2 and 4 of the phenyl ring afforded highly potent and completely selective ligands (**11k**, **12k**, and **13k**) toward the A_3AR subtype, regardless of the alkylic residue present in the amide group at position 4 of the heterocyclic backbone. Finally, in a clear contrast with the results described so far, replacement of the phenyl group in the parent compounds by heterocyclic cores proved to be highly discouraging, generating a series of potent but nonselective ligands.

An integrated analysis of the data presented in Table 2 for the 4-amide homologous series (compounds **11**−**13**) is shown in Figure 4. In this representation the experimental K_i values at hA_3AR are plotted as a function of both the L1 and the L2/L3 substitutions. The weak modulator effect exerted by the alkyl residues of the amide functions (L1) on the activity/selectivity profile within these series can be observed. It can be clearly appreciated that the size of L1 is inversely correlated with the affinity within each subseries, an observation that is consistent with previous findings.[38] Moreover, a detailed inspection of the pharmacological data reported for these series (Table 2) shows that A_3AR selectivity also increases on reducing the size of the L1 substituent. Only some combinations of L2/L3 substituents show little sensitivity to the nature of the L1 substituent, in particular, compounds incorporating 4-methoxyphenyl (**11d**, **12d**, **13d**) or 2,4-dimethoxyphenyl (**11k**, **12k**, **13k**) residues (i.e., the substituent present in compounds eliciting the highest affinity).

Once the initial hypothesis that hA_3AR could be more tolerant to bulky L2/L3 substituents had been validated by the SAR data, an exhaustive molecular modeling study was developed to gain new insights into the structure−affinity relationship for the hA_3AR. A homology model of the hA_3AR receptor was built using the recently crystallized hA_{2A}AR structure as a template. This model served as a basis for an automated docking exploration of the 64 compounds for which experimental K_i values at the hA_3AR are reported. The choice of the docking algorithm (GOLD program in combination with the Chemscore scoring function)[55] is the result of an internal validation of different docking alternatives in order to reproduce the experimental binding pose of 4-(2-[7-amino-2-(2-furyl)[1,2,4]triazolo[2,3-*a*][1,3,5]triazin-5-ylamino]ethyl)phenol/hA_{2A}AR (data not shown), a validation that is in agreement with a recent comparative study of ligand docking tools in ARs.[49] The systematic docking exploration identified one conserved binding mode for both regioisomeric diaryl amidopyrimidine series reported here. This binding mode was found in 62 of the 64 compounds (97% of the cases), and this mode was the top scored pose by Chemscore in 66% of the cases. Moreover, in 63% of the cases, this binding pose was the most populated according to an rmsd tolerance of 1 Å for the clustering. This binding mode is represented in Figure 5 for compound **11d**.

The main anchoring point is a double hydrogen bond of the exocyclic amino/amido group (donating) and its closest nitrogen atom in the pyrimidine ring (N3, accepting) with Asn 6.55 (note the Ballesteros−Weinstein residue numbering[56]), a totally conserved residue of the adenosine receptor family. At the same time, the pyrimidine ring is flanked by the side chain of Phe 5.29, in the second extracellular loop (EL2), and Leu 6.51 in helix 6. This interaction pattern of the aminopyrimidine moiety (π-stacking with Phe 5.29, hydrophobic interactions with Leu 6.51 and hydrogen bonding to Asn 6.55) resembles the experimentally observed binding mode of 4-(2-[7-amino-2-(2-furyl)[1,2,4]triazolo[2,3-*a*][1,3,5]triazin-5-ylamino]ethyl)phenol with the hA_{2A}AR.[47] Accordingly, the important role in ligand binding of residues 5.29 and 6.51 has recently been validated in a site-directed mutagenesis study of the A_{2A}AR.[57] Interestingly, Phe 5.29 is totally conserved in the ARs family, while Leu 6.51 is substituted by a smaller valine in the low-affinity hA_{2B}AR, and the replacement of this residue by an alanine in hA_{2B}AR completely abolishes ligand binding.[57] As far as position 6.55 is concerned, there is biochemical evidence that suggests the important role of this residue in ligand binding for several ARs, including the A_3AR.[58−60] The molecular alignment of the 62 molecules, obtained by ligand-docking, is shown in Figure 6. It can be appreciated that the volume of the L1 and L2 subsites has been

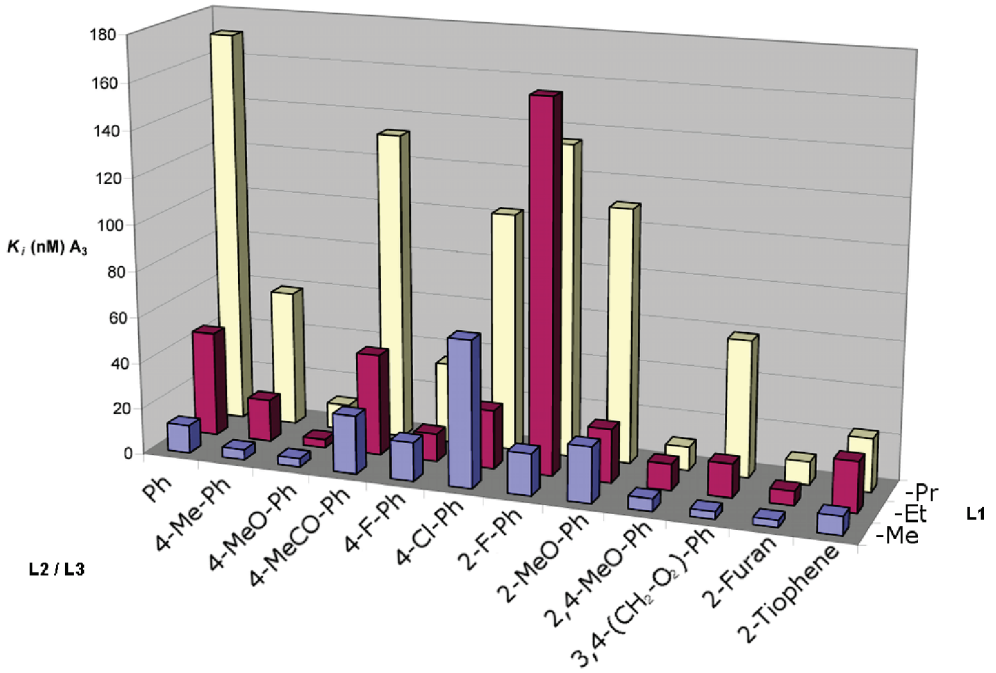

Figure 4. Effect of the nature of the L1 substituent on the human A_3 adenosine receptor affinity for the series of 2,6-diaryl-4-amidopyrimidines. The figure only represents those compounds that have experimental K_i for the three considered L1 substitutions.

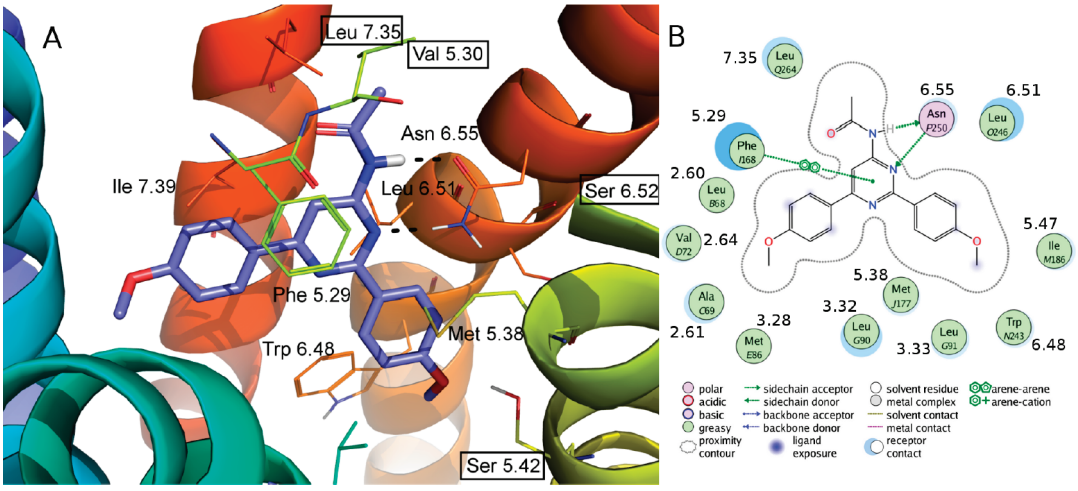

Figure 5. Binding mode of compound **11d**, showing the main receptor−ligand interactions. Residues that are specific for the human A_3 adenosine receptor are shown in boxes in the 3D panel (A), generated in PyMol (http://www.pymol.org). The double hydrogen bond with Asn 6.55 is indicated by dashed lines. Panel B shows a schematic representation of residue−ligand interactions, calculated with LigX as implemented in MOE. Residues are labeled according to the Ballesteros & Weinstein numbering.[56]

well explored, while there is a volume tolerance in the subsite occupied by L3 (helices 2, 3, 7) that was not completely explored by our ligand series. Even after one energy minimization cycle, the molecular alignment did not change substantially and the highest variability is still located on the L3 site.

This molecular alignment was the basis for a 3D-QSAR study that involved the use of the new generation of GRid-INdependent Descriptors (GRIND-2).[50,51] The first generation of these molecular interaction field (MIF)-based descriptors was originally conceived precisely to circumvent the necessity of obtaining a highly accurate molecular alignment of the molecules prior to the 3D-QSAR analysis.[61] However, the most recent version of the GRIND methodology includes a new mathematical transformation applied to the MIF descriptors that guarantees that a given variable represents exactly the same information for every compound of the series.[51] This method, called consistency large auto and cross correlation (CLACC), either generates a molecular alignment of the molecules, on the basis of the correlation of the variables, or either it uses an input molecular alignment provided by the user (e.g., obtained by molecular docking). The first (default) option is recommended for the exploration of compounds that have closely related structures, while the second approach (docking alignment) is a good compromise for series that present problems with the CLACC alignment. An advantage of the last option is that the interpretation of the derived models can be easily expressed in the context of receptor−ligand interactions, allowing it to retrieve structural information on the binding site. We explored all of these different settings for the generation of 3D-QSAR models, the

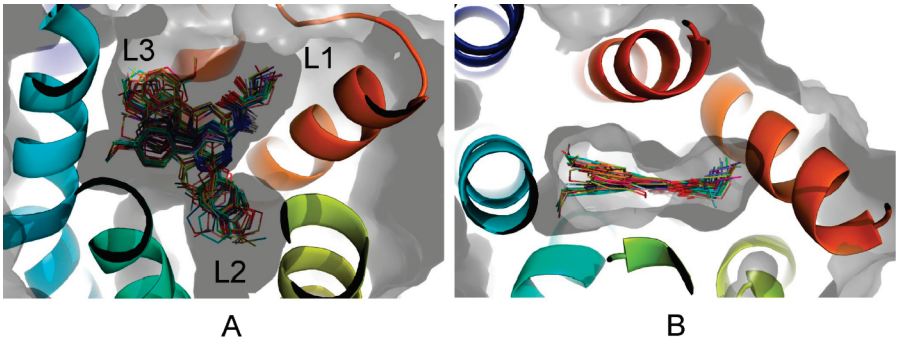

Figure 6. Molecular alignment of the 62 molecules that had the postulated docking pose. This alignment was used as an input for the 3D-QSAR study. (A) side view of the receptor, and (B) view from the extracellular side. The following transmembrane helices (TM) are shown: TM2 (cyan), TM3 (green), TM4 (yellow), TM6 (orange), and TM7 (red). The Connolly surface of the receptor is depicted in gray.

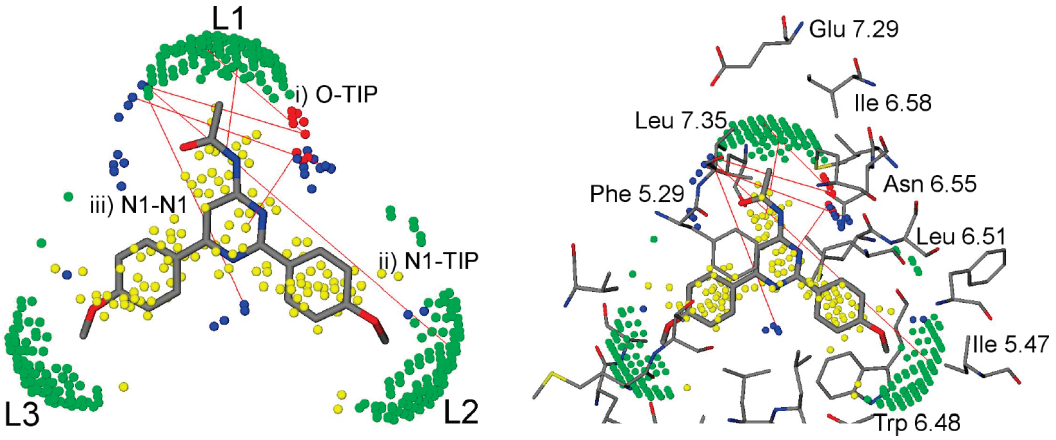

Figure 7. Important variables in the 3D-QSAR model C (represented for compound **11d**). Green dots denote TIP fields, red dots O fields, blue dots N1 fields, and yellow dots DRY fields. (Right) The same representation showing the binding site. The correspondence of the TIP fields with the limiting pockets of the receptor for the L1 (Glu 7.29, Ile 7.35) and L3 (Ile 5.47, Trp 6.48), the superposition of the O−NI short distance variable with Asn 6.55, and the DRY field with Phe 5.29 can be appreciated.

results being summarized in Table S1 of the Supporting Information. The model generated on the basis of a docking molecular alignment and the CLACC method for encoding the descriptors (*Model C* in Table S1, Supporting Information) was selected for further interpretation. This 3D-QSAR model has two latent variables (LV) and presents a satisfactory statistical quality, with a fitting parameter of $r^2 = 0.86$ and a predictive ability of $q^2 = 0.67$, as obtained by the LOO cross-validation test. The standard error for the correlation and the prediction was 0.31 and 0.48 pK_i log units, respectively.

The interpretation of the model highlights the key structural features for high A_3AR affinity. The most important variables, that is, those with the highest PLS positive coefficients, were used for the model interpretation and are depicted in Figure 7. These variables represent, in an ideal case, structural features that are present in the active compounds but absent in the inactive compounds. In this respect, the following features are important for the model interpretation:

(i) The hydrophobic interactions at the extracellular tip of the binding site, mainly with residues Ile 6.58 and Leu 7.35, are identified with the O-TIP (optimum distance at 5.8 Å) and the DRY-TIP (6.6 Å) correlograms. These two hydrophobic residues are a probable source of A_3 specificity: position 6.58 is occupied by a threonine in the other subtypes, while position 7.35 has already been related to interspecies selectivity in the A_1AR.[63] The model suggests that an optimal shape complementarity is achieved by molecules with smaller L1 substituents (e.g., acetamides) or, alternatively, molecules bearing larger L1 substituents but smaller L2/L3 substituents (e.g., **13n**). The combination of the aforementioned descriptors provides information about the interdependence of the size of L1 and L2/L3 substituents. This descriptor also accounts for the lack of affinity observed in the aminopyrimidine series (see Table 1), since these scaffolds do not bear any alkyl residues on the exocyclic nitrogen.

(ii) The optimal pharmacophoric distance between the H-bond acceptor probe, corresponding to the carbonyl of the amide, and the shape of the L2 substituent is located at 16.6 Å in the N1-TIP cross-correlogram. Whereas the role of the carbonyl group could be hypothesized as a water-mediated interaction with Glu 7.29 in the third extracellular loop (EL3), this descriptor mainly identifies the importance of residue Ile 5.47, interacting with the L2 substituent. Importantly, Ile 5.47 is occupied by the less bulky valine in the other AR subtypes, a fact that could be taken into account to improve A_3 selectivity.

(iii) Finally, the O−N1 and N1−N1 autocorrelograms account for the differences between the 2-amido- or 4-amidopyrimidine series, since these molecular descriptors identify the distances between the exocyclic amide and the N1 in the ring. In the series of

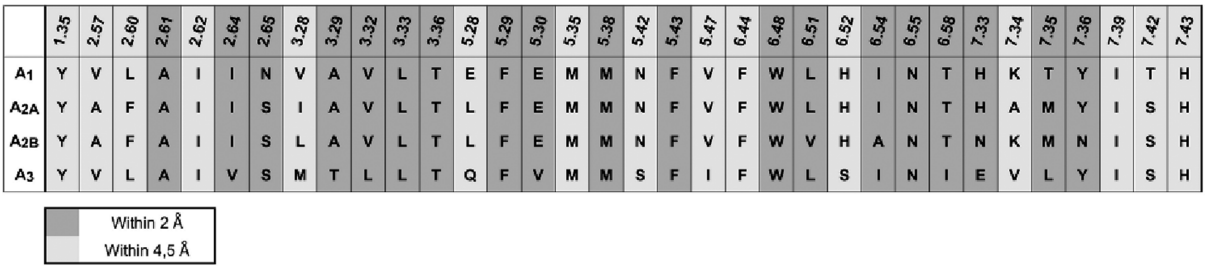

Figure 8. Multiple pseudosequence alignment of human ARs, taking hA_3AR residues within 4.5 Å of all docked compounds into account. Residue positions are denoted by the Ballesteros & Weinstein numbering,[56] and shaded in gray according to their distance toward the docked compounds.

4-amidopyrimidines, optimum distances of 9 and 10.6 Å for O−N1 and N1−N1 autocorrelograms, respectively, are observed. Conversely, in the series of 2-amidopyrimidines, a descriptor in the N1−N1 correlogram, which is negatively related with affinity in the model, identifies the particular location of the N1 of this scaffold closer to the carbonyl of the amide (distance 4.6 Å).

This last point is intriguing, since the docking model does not identify any polar interaction for either the oxygen of the amide group or the nitrogen at position N1 of the pyrimidine (i.e., the nitrogen that varies in position between 2- and 4-amidopyrimidines). However, if we compare the binding mode of the molecular series here reported on the A_3AR with the experimental binding mode of 4-(2-[7-amino-2-(2-furyl)-[1,2,4]triazolo[2,3-*a*][1,3,5]triazin-5-ylamino]ethyl)phenol on the $A_{2A}AR$, it appears that the N1 in the 4-amidopyrimidines series overlies with a nitrogen in the heterocycle of the standard (N19 according to PDB nomenclature in entry 3EML).[47] Recently, the group of Jacobson[63] noted the importance of a polar interaction of this N19 with crystallographic water molecules. In order to check if similar interactions could be achieved in our 4-amidopyrimidines/hA_3AR complexes, we performed a computational exploration of structural water molecules in the binding site of the hA_3AR model, as detailed in the methods section. The results (Figure S2, Supporting Information) show an energetically favorable area for a water molecule that overlaps with the N1−N1 descriptor, close to the position of the varying nitrogen in the 4-amidopytimidines (blue dots at the bottom of Figure 7). A water-mediated interaction between N1 and Thr 7.42, which somehow resembles the H-bond network ZM24-1386(N19)-HOH^{559}-HOH^{550}-His7.43(Nε) in the $A_{2A}AR$, is thus proposed as an specific polar contact for the 4-amidopyrimidine series, lacking in the 2-amidopyrimidines. The experimental validation of such a different interaction behavior is currently being investigated in our laboratory by synthesizing additional series of unexplored heterocyclic scaffolds.

As stated above, an advantage of the 3D-QSAR methodology employed in this study is to place the relevant descriptors in the context of the binding site. This procedure can not only deal with the structural requirements of the hA_3AR for high affinity but also enables a comparison of the hot-spots with the relative positions in other ARs in order to explore the reasons for selectivity. In an effort to identify these hot-spots, we built a so-called "pseudosequence" based on the docking results of this study. This pseudosequence is defined by all of the residues of the receptor located at a a maximum distance of 4.5 Å from the most exposed atom of the group of ligands docked in the hA_3AR (as superimposed in Figure 6). An alignment of this pseudosequence for the human members of the ARs family is shown in Figure 8, in which the variable positions are clearly identified.

In this respect, it is remarkable that positions 5.42 and 6.52, at the bottom edge of the binding site, are both occupied by a serine in the hA_3AR (see Figure 5); in the other three human ARs these positions are occupied by Asn 5.42 and His 6.52, respectively. The less voluminous side chain of a serine in these positions would allow the accommodation of bulkier L2 substituents in this subsite at the hA_3AR, thus offering a rationale for the observed receptor selectivity. There are also remarkable differences within the ARs family regarding residues at the top of the binding site: Ile 6.58, interacting with L1, is replaced by a smaller valine in the other ARs. hA_3AR presents a valine at position 5.30 (in the tip of EL2), which replaces a Glu that is conserved in the other three hAR subtypes. According to the $A_{2A}AR$ crystallographic structure, Glu 5.30 hydrogen bonds with the side chain of a His 7.29 in EL3, thus closing the top of the binding site while accepting an additional hydrogen bond from the amino group of 4-(2-[7-amino-2-(2-furyl)[1,2,4]triazolo[2,3-*a*][1,3,5]triazin-5-ylamino]ethyl)phenol.[47] The amino derivatives would benefit from this interaction, thus explaining the low selectivity profile displayed by this group of compounds (Table 1). Interestingly, a recent study of a new series of 2-phenylpyrazolo[4,3-*d*]pyrimidin-7-ones already indicated this difference in the flap regions as being responsible for the A_3AR selectivitiy.[49] Finally, Leu 7.35 provides a specific hydrophobic subsite for the L1 substituent compared to the more voluminous methionine present at this position in the $A_{2A}AR$ and $A_{2B}AR$ or the polar Thr 7.35 in A_1AR. Importantly, site directed mutagenesis studies have identified this position as being responsible for the interspecies differences in ligand affinities in the A_1ARs.[62]

To further challenge the computational model in terms of robustness and predictive capability, the tolerance of A_3AR to steric factors imposed by the alkyl residue of the amide function (L1) was explored. Accordingly, six compounds were designed which combined three new bulky residues [e.g., $CH(Me)_2$, $CH(Et)_2$, and Cy] on the exocyclic amide group with the scaffold of the amines **4d** and **4k**. The compounds were docked on the A_3AR and queried to the QSAR model, which predicted a good affinity profile for the A_3AR (see Table 3). Figure S2 in the Supporting Information shows how the most bulky compounds (**14c** and **14f**) optimally accommodate the cyclohexyl substituent in the hA_3AR pocket. On the other hand, a superposition with the crystallographic structure of the $hA_{2A}AR$ shows that steric clashes with the L1 substituent of this receptor might occur, as anticipated by the pseudosequence analysis shown in Figure 8. The compounds

Table 4. Structure and Affinity Binding Data for 2,6-Diaryl-4-amidopyrimidines **14** at the Human Adenosine Receptors

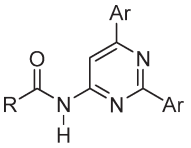

			K_i (nM) or % at 0.1 μM				pK_i @ hA_3	
comp	Ar	R	hA_1[a]	hA_{2A}[b]	hA_{2B}[c]	hA_3[d]	exp	pred
14a	4-OMe-Ph	$CH(Me)_2$	5%	1%	3%	12.2 ± 0.9	7.91	8.16
14b		$CH(Et)_2$	3%	6%	8%	58.1 ± 4.7	7.24	7.82
14c		Cy	5%	1%	1%	32.1 ± 2.4	7.49	7.15
14d	2,4-OMe-Ph	$CH(Me)_2$	18%	1%	1%	15.9 ± 1.3	7.8	7.58
14e		$CH(Et)_2$	1%	2%	2%	52.4 ± 6.2	7.28	7.57
14f		Cy	1%	1%	4%	56.3 ± 6.1	6.59	6.85

[a] Displacement of specific [^{3}H]DPCPX binding in human CHO cells expressed as K_i ± SEM in nM ($n = 3$) or percentage displacement of specific binding at a concentration of 0.1 μM ($n = 2$). [b] Displacement of specific [^{3}H]4-(2-[7-amino-2-(2-furyl)[1,2,4]triazolo[2,3-*a*][1,3,5]triazin-5-ylamino]-ethyl)phenol binding in human HeLa cells expressed as K_i ± SEM in nM ($n = 3$) or percentage displacement of specific binding at a concentration of 0.1 μM ($n = 2$). [c] Displacement of specific [^{3}H]DPCPX binding in human HEK-293 cells expressed as K_i ± SEM in nM ($n = 3$) or percentage displacement of specific binding at a concentration of 0.1 μM ($n = 2$). [d] Displacement of specific [^{3}H]NECA binding in human HeLa cells expressed as K_i ± SEM in nM ($n = 3$) or percentage displacement of specific binding at a concentration of 0.1 μM ($n = 2$).

were then prepared and tested at the four human adenosine receptor subtypes (Table 4). As predicted by the computational exploration described above, the newer derivatives exhibit potent and selective activity profiles, which unequivocally confirms the tolerance of hA_3AR to the size of the L1 substituent. Excellent agreement is found between predicted and experimental affinity values for the six compounds designed and tested in this part of the study [with an impressive low standard error of the prediction (SDEP = 0.37 log pK_i units)], which further confirms the predictive power of the integrated computational model reported in this work, that is, combining a molecular alignment from automated docking with the prediction of activities on the basis of the 3D-QSAR model (see Supporting Information, Figure S3C) was observed. It is worth noting that on the solely basis of the available literature[39] data or the herein established SAR (Tables 1 and 2) the synthesis of compounds **14** would not have been advisible. Thus, the modeling exploration enabled us to anticipate attractive activity/selectivity profiles for compounds incorporating hindered fragments at the amide chain (as consequence of the higher tolerability for the L1 subsite of the hA_3AR).

Conclusions

A new series of structurally simple and highly potent ligands that exhibit remarkable selectivity profiles toward the A_3AR has been identified. A previous series of potent and selective A_1AR antagonists was selected, and the subsequent stepwise structural diversification of these model substrates was carried out in order to radically modify the activity/selectivity profiles while simultaneously providing valuable structural information on the requirements for its binding at the hA_3 receptor subtype. Excellent affinity toward the hA_3AR ($K_i \leq 6$ nM) and optimal selectivity profiles ($\leq 10\%$ displacement of 0.1 μM concentrations at the other ARs) were observed for compounds **ISVY133**, **ISVY130**, **ISVY074**, and **ISVY167**, which incorporate 4-tolyl, 4-methoxyphenyl, and 2,4-dimethoxyphenyl moieties at the 2,6-positions of the heterocyclic backbone. The antagonistic behavior of five representative derivatives of these series was unequivocally validated through functional cAMP experiments. The main SARs identified were substantiated by an exhaustive molecular modeling study that combined a receptor-driven docking model, which was constructed on the basis of the recently published crystal structure of the $hA_{2A}AR$, and a ligand-based 3D-QSAR model, highlighting the key structural features required for the optimal interaction with the hA_3 receptor subtype in these compounds. The robustness and predictive capabilities of the model were validated by designing novel series of compounds that explore new alkyl residues at the L1 subsite, which show high affinity and selectivity profiles for the hA_3AR. We must note that these compounds would not have been synthesized solely on the basis of the available SAR data on the literature[39] or the qualitative SAR established on this work (Tables 1−3). On the contrary, the interest of these compounds was envisioned by the computational modeling exploration, suggesting that the hA_3AR shows higher tolerability for the L1 subsite. Further experiments are currently in progress in our laboratories to prepare new libaries incorporating nonidentical aryl groups at positions 2,6 and 4,6 obtained by adaptation of the herein documented synthetic strategy according to recently published methodologies.[64−66] The biological profile of these new derivatives will be published in due course.

Experimental Section

Chemistry. Commercially available starting materials, reagents, and solvents were purchased (Sigma-Aldrich) and used without further purification. When necessary, solvents were dried by standard techniques and distilled. After being extracted from aqueous phases, the organic solvents were dried over anhydrous sodium sulfate. The reactions were monitored by thin-layer chromatography (TLC) with 2.5 mm Merck silica gel GF 254 strips, and the purified compounds each showed a single spot; unless stated otherwise, UV light and/or iodine vapor were used for detection of compounds. The Suzuki cross-coupling reactions were performed in coated Kimble vials on a PLS (6 × 4) Organic Synthesizer with orbital stirring. Filtration and washing protocols for supported reagents were performed in a 12-channel vacuum manifold from Aldrich. Purity and identity of all tested compounds were established by a combination of HPLC, elemental analysis, mass spectrometry, and NMR spectra as described below. Purification of isolated products was carried out by column chromatography (Kieselgel 0.040−0.063 mm, E. Merck) or

Table 5. Conditions Used for Radioligand Binding Assays Using A_1, A_{2A}, A_{2B}, and A_3 Human Adenosine Receptors

	A_1	A_{2A}	$2A_{2B}$	A_3
Buffer A	20 mM Hepes, 100 mM NaCl, 10 mM $MgCl_2$, 2 units/mL adenosine deaminase (pH = 7.4)	50 mM Tris-HCl, 1 mM EDTA, 10 mM $MgCl_2$, 2 units/mL adenosine deaminase (pH = 7.4)	50 mM Tris-HCl, 1 mM EDTA, 10 mM $MgCl_2$, 0.1 mM benzamidine, 2 units/mL adenosine deaminase (pH = 6.5)	50 mM Tris-HCl, 1 mM EDTA, 5 mM $MgCl_2$, 2 units/mL adenosine deaminase (pH = 7.4)
Buffer B	20 mM Hepes, 100 mM NaCl, 10 mM $MgCl_2$, (pH = 7.4)	50 mM Tris-HCl, 1 mM EDTA, 10 mM $MgCl_2$ (pH =7.4)	50 mM Tris-HCl (pH = 6.5)	50 mM Tris-HCl (pH = 7.4)
plate	GF/C	GF/C	GF/B	GF/B
radioligand	[^{3}H]DPCPX nM	[^{3}H]ZM2413853 nM	[^{3}H]DPCPX35 nM	[^{3}H]NECA 30 nM
nonspecific binding	10 μM (R)-PIA	50 μM NECA	400 μM NECA	100 μM (R)-PIA
incubation	25 °C/60 min	25 °C/30 min	25 °C/30 min	25 °C/180 min

medium pressure liquid chromatography (MPLC) on a Combi-Flash Companion (Teledyne ISCO) with RediSep prepacked normal-phase silica gel (35−60 μm) columns followed by recrystallization. Melting points were determined on a Gallenkamp melting point apparatus and are uncorrected. The NMR spectra were recorded on Bruker AM300 and XM500 spectrometers. Chemical shifts are given as δ values against tetramethylsilane as internal standard and J values are given in Hz. Mass spectra were obtained on a Varian MAT-711 instrument. High resolution mass spectra were obtained on an Autospec Micromass spectrometer. Analytical HPLC was performed on a Agilent 1100 system using an Agilent Zorbax SB-Phenyl, 2.1 mm × 150 mm, 5 μm column with gradient elution using the mobile phases (A) H_2O containing 0.1% CF_3COOH and (B) MeCN and a flow rate of 1 mL/min. Elemental analyses were performed on a Perkin-Elmer 240B apparatus at the Microanalysis Service of the University of Santiago de Compostela, the elemental composition of the new compounds agreed to within ±0.4% of the calculated value. The purity of all tested compounds was determined to be >95%. A detailed description of synthetic methodologies as well as analytical and spectroscopic data for all described compounds is included in the Supporting Information.

Pharmacology. Radioligand binding competition assays were performed in vitro as previously described[53] using A_1, A_{2A}, A_{2B}, and A_3 human adenosine receptors expressed in transfected CHO (A_1AR), HeLa (A_{2A}AR and A_3AR), and HEK-293 (A_{2B}AR) cells. The experimental conditions used are summarized in Table 5. In each instance, aliquots of membranes (15 μg for A_1, 10 μg for A_{2A}AR, 18 μg for A_{2B}AR, and 90 μg for A_3AR) in buffer A (see Table 5) were incubated for the specified period at 25 °C with the radioligand (2−35 nM) and six different concentrations (ranging from 0.1 nM to 1 μM) of the test molecule in a final volume of 200 μL. The binding reaction was stopped by rapid filtration in a multiscreen manifold system (Milipore Ibérica, Madrid, Spain). Unbound radioligand was removed by washing four times with 250 μL of ice-cold buffer B for A_1 and A_{2A} receptors, and six times with 250 μL of ice-cold buffer B for A_{2B}AR and A_3AR (see Table 5). Nonspecific binding was determined using a 50 or 400 μM NECA solution for A_{2A}AR and A_{2B}AR and 10 or 100 μM R-PIA solution for A_1AR and A_3AR, respectively. Radioactivity retained on filters was determined by liquid scintillation counting using Universol (ICN Biochemicals, Inc.). The binding affinities were determined using [^{3}H]-DPCPX (130 Ci/mmol; GE-Healthcare, Barcelona, Spain) as the radioligand for A_1AR and A_{2B}AR, [^{3}H]4-(2-[7-amino-2-(2-furyl)[1,2,4]triazolo[2,3-*a*][1,3,5]triazin-5-ylamino]ethyl)phenol (21 Ci/mmol; Tocris, Madrid, Spain) for A_{2A}AR and [^{3}H]-NECA (15.3 Ci/mmol; NEN-Perkin-Elmer Life Sciences, Madrid, Spain) for A_3AR.

The inhibition constant (K_i) of each compound was calculated by the expression: $K_i = IC_{50}/(1 + (C/K_D))$; where IC_{50} is the concentration of compound that displaces the binding of radioligand by 50%, C is the free concentration of radioligand, and K_D is the apparent dissociation constant of each radioligand. The percentage of displacement of specific binding was calculated by the expression: % of displacement = ((BT − dpm)*100)/(BT − NSB); where BT is the total binding of the radioligand in the assay, NSB is the nonspecific binding of the radioligand in the assay, and dpm are the radioactive measurements obtained by competing the radioligand binding with a given concentration of the test compound. Unless otherwise specified, results shown in the text and tables are expressed as means ± SEM. Significant differences between two means ($p < 0.05$ or $p < 0.01$) were determined by one-way analysis of variance (ANOVA) and/or by Student's t test for nonpaired data.

Molecular Modeling

Model Building. A homology model of the hA_3AR was built using the recently crystallized hA_{2A}AR as a template. The modeling protocol is adapted from our participation in the GPCR Dock 2008 competition.[44] Briefly, a sequence alignment between the two receptors with Clustal (PAM250 substitution matrix, with open and elongation gap penalties of 10 and 0.05)[67] was provided to Modeller v9.4.[68] Fifteen initial models were obtained using standard parameters. In a first stage, the best five models were selected on the basis of Procheck[69] geometrical quality and DOPE scoring, and these were subjected to geometrical improvement by the Molprobity server.[70] In a second stage, the best model from the previous step was subjected to loop optimization with the LoopModel routine in Modeler,[71] again generating 15 refined models. We selected the best model on the basis of a compromise between Procheck stereochemical quality and the DOPE energetical ranking. The geometry of the loops in the selected model was refined by partial energy minimization (i.e., nonloop residues were frozen) using the Polak−Ribiere algorithm (convergence criteria 0.05 kcal/mol·Å^2) and the OPLS-AA force-field as implemented in Macromodel.[72] The general numbering scheme for GPCRs proposed by Ballesteros and Weinstein[56] was adopted through this work. In essence, every residue is numbered as X.YY, where X corresponds to the transmembrane helix (X = [1,7]) and YY is a correlative number in the protein sequence, but taking as a reference position (YY = 50) the most conserved residue in the given helix.

Protein−Ligand Docking. Automated docking exploration was performed with GOLD version 3.2.[73] Each ligand was docked 20 times with default (high accuracy) genetic algorithm (GA) search parameters, using the scoring function Chemscore as implemented in GOLD[55] and allowing full flexibility for the ligand, including flipping of amide bonds. The search sphere was centered on the side chain (CD1) of Ile 7.39, and expanded with a radius of 15 Å, thus ensuring a generous enough search space comprising the

antagonist binding site experimentally determined for adenosine receptors.[46] The criterion for the selection of docking poses was based on Chemscore ranking and the population of the solutions (according to a clustering criteria of 1 Å).

Geometrical Optimization. Each docking pose was refined by partial energy minimization of the binding site with MOE.[74] The site was selected as any atom within a distance of 4.5 Å around the ligand and OPLS-AA parameters were used in combination with GBSA model for continuum solvent representation. The convergence criterion for the steepest descendent algorithm was set to 0.01 rmsd.

3D-QSAR. The conformations of the compounds obtained in the molecular docking step were used to generate a 3D-QSAR model with the software Pentacle v1.1.[75] This software allows the computation of the second generation of GRid Independent Descriptors (GRIND-2). This family of molecular descriptors, which are widely used in QSAR studies, are generated in a three-step fashion: (i) computation of molecular interaction fields (MIF) with different Grid probes,[76] (ii) selection of the most relevant MIF nodes, and (iii) encoding of the descriptors as alignment-independent vectors of node pairs, obtaining the so-called correlograms.[61] The advantages of GRIND-2 include the use of AMANDA as a new discretization algorithm for the identification of "hot spots" (most relevant MIF nodes)[50] and a new method for encoding descriptors into alignment-free vectors called CLACC.[51] This method detects consistency in the computed variables, ensuring that a given vector on the correlogram corresponds to the description of same pharmacophoric property within the series. In this work, the MIF were computed using default values (i.e., GRID probes: DRY, O, N1, TIP; 0.5 Å grid step; dynamic parametrization), discretization was carried out with default AMANDA parameters and the CLACC encoding of the variables was generated on the basis of the docking alignment ("use CLACC for alignment" = false) with strict options, meaning that any variable that is not consistent in the series is removed ("Remove non-consistent couples" = true). Two rounds of fractional factorial design (FFD) were applied for the selection of the most relevant variables in the model. The model generated was "saved for predictions" through the corresponding menu option in Pentacle. Thereafter, the designed molecules were docked in the A_3 receptor as explained above, and further imported in the Pentacle software, but using the generated model as a template for the prediction of activities on the A_3 receptor.

Water Analysis. The prediction of energetically favorable regions for structural water molecules in the binding site of the hA_3AR model was carried out with the program Grid,[76] using the following parameters: OH2 probe, all program directives on their default values except for LEAU = 2 and NPLA = 2. Further refinement of the position of predicted water molecules was done with the module FilMap, as implemented in the Grid software.

Acknowledgment. This work has been developed in the frame of the Red Gallega de Investigación y Desarrollo de Medicamentos (REGID) and was financially supported by the Fondo Europeo de Desarrollo Social (FEDER) and the Galician Government (Projects 09CSA016234PR and PS09/63). E.S. is the recipient of a Consolidation Group Research Grant from the Conselleria de Educación (Xunta de Galicia). E.S., H.G.d.T., and A.C. are researchers of the Isidro Parga Pondal program (Xunta de Galicia, Spain). J.B. is researcher of the Isabel Barreto program (Xunta de Galicia, Spain). D.R. is recipient of a PFIS grant from the Instituto de Salud Carlos III (Ministerio de Ciencia e Innovación, Spain). We are grateful to Dr. Manuel Pastor for assistance in the use of the Pentacle software and helpful discussions.

Supporting Information Available: Experimental details for the synthesis of compounds described, the spectroscopic, spectrometric, and elemental analysis data of all compounds prepared as well as additional molecular modeling details. This material is available free of charge via the Internet at http://pubs.acs.org.

References

(1) Fredholm, B. B.; Arslan, G.; Halldner, L.; Kull, B.; Shulte, G.; Wasserman, W. Structure and function of adenosine receptors and their genes. *Naunyn-Schmiedeberg's Arch. Pharmacol.* **2000**, *362*, 364–374.
(2) Murphree, L. J.; Linden, J. Adenosine receptors. *Encyclopaedia Biol. Chem.* **2004**, *1*, 34–39.
(3) Jacobson, K. A.; Knutsen, L. J. S. P1 and P2 purine and pyrimidine receptor ligands. In *Purinergic and Pyrimidine Signalling* (*Handbook of Experimental Pharmacology*); Abbrachio, M., Williams, M., Eds.; Springer: Berlin, 2001; Vol. 151/1, pp 129−175.
(4) Fredholm, B. B.; Ijzerman, A. P.; Jacobson, K. A.; Koltz, K. N.; Linden, J. International union of pharmacology XXV. Nomenclature and classification of adenosine receptors. *Pharmacol. Rev.* **2001**, *53*, 527–552.
(5) Baraldi, P. G.; Aghadeh, M.; Tabrizi, M. A.; Gessi, S.; Borea, P. A. Adenosine receptor antagonists: translating medicinal chemistry and pharmacology into clinical utility. *Chem. Rev.* **2008**, *108*, 238–263.
(6) Jacobson, K. A.; Gao, Z. Adenosine receptors as therapeutic targets. *Nat. Rev. Drug Discovery* **2006**, *5*, 247–264.
(7) Moro, S.; Gao, Z. G.; Jacobson, K. A.; Spalluto, G. Progress in the pursuit of therapeutic adenosine receptor antagonists. *Med. Res. Rev.* **2006**, *26*, 131–159.
(8) Zhou, G. L.; Olah, M. E.; Johnson, R. A.; Stiles, G. L.; Clivelli, O. Molecular cloning and characterization of an adenosine receptor: the A_3 adenosine receptor. *Proc. Natl. Acad. Sci. U. S. A.* **1992**, *89*, 7432–7436.
(9) Van Schaick, E. A.; Jacobson, K. A.; Kim, H. O.; IJzerman, A. P.; Danhof, M. Hemodynamic effects and histamine release elicited by the selective adenosine A_3 receptor agonist Cl-IB-MECA in conscious rats. *Eur. J. Pharmacol.* **1996**, *308*, 311–314.
(10) Hannon, J. P.; Pfannkuche, H. J.; Fozard, J. R. A role for mast cells in adenosine A_3 receptor-mediated hypotension in the rat. *Br. J. Pharmacol.* **1995**, *115*, 945–952.
(11) Fishman, P.; Bar-Yehuda, S. Pharmacology and therapeutic applications of A_3 receptor subtypes. *Curr. Top. Med. Chem.* **2003**, *3*, 463–469.
(12) Muller, C. E. A_3 Adenosine receptor antagonists. *Mini Rev. Med Chem.* **2001**, *1*, 417–427.
(13) Baraldi, P. G.; Tabrizi, M. A.; Fruttarolo, F.; Borevo, A.; Avitabile, B.; Preti, D.; Romagnoli, R.; Merighi, S.; Gessi, S.; Varani, K.; Borea, P. A. Recent developments in the field of A_3 adenosine receptor antagonists. *Drug Dev. Res.* **2003**, *58*, 315–329.
(14) Baraldi, P. G.; Fruttarolo, F.; Tabrizi, M. A.; Romagnoli, R.; Preti, D.; Carrion, M.; Iaconinoto, A.; Borea, P. A. Recent improvements in the field of A_3 adenosine receptor ligands. *Exp. Opin. Ther. Pat.* **2005**, *15*, 1507–1519.
(15) Muller, C. E. Medicinal chemistry of adenosine A_3 receptor ligands. *Curr. Top. Med. Chem.* **2003**, *3*, 445–462.
(16) Moro, S.; Deflorian, F. Novel strategies for the design of new potent A_3 antagonists: an update. *Curr. Med. Chem.* **2006**, *13*, 639–645.
(17) Baraldi, P. G. A_3 ligands, history and perspectives. *Med. Res. Rev.* **2000**, *20*, 103–128.
(18) Van Muijlwijk-Koezen, J. E.; Timmerman, H.; Ijzerman, A. P. The adenosine A_3 receptor and its ligands. *Prog. Med. Chem.* **2001**, *38*, 61–113.
(19) Stone, T. W. Purines and neuroprotection. *Adv. Exp. Med. Biol.* **2002**, *513*, 249–280.
(20) Beaven, M. A.; Ramkumar, V.; Hydar, A. Adenosine A_3 receptors in mast cells. *Trends Pharmacol. Sci.* **1994**, *15*, 13–14.

(21) Ramkumar, V.; Stiles, G. L.; Beaven, M. A.; Ali., H. The A_3 adenosine receptor is the unique adenosine receptor which facilitates release of allergic mediators in mast cells. *J. Biol. Chem.* **1993**, *268*, 16887–16890.
(22) Akkari, R.; Burbiel, J. C.; Hockemeyer, J.; Mueller, C. E. Recent progress in the development of adenosine receptor ligands as antiinflammatory drugs. *Curr. Top. Med. Chem.* **2006**, *6*, 1375–1399.
(23) Von Lubitz, D. K. J. E.; Carter, M. F.; Deutsch, S. I.; Lin, R. C. S.; Mastropaola, J.; Meshulam, Y.; Jacobson, K. A. The effects of adesnosine receptor stimulation on seizures in mice. *Eur. J. Pharmacol.* **1995**, *275*, 23–29.
(24) Nieber, K.; Lewerenz, A.; Hentschel, S.; Vissiennon, Z. Adenosine A_1 and A_3 receptors: Neuroprotective targets with perspectives. *Bioforum* **2002**, *25*, 237–240.
(25) Forsythe, P.; Ennis, M. Adenosine, mast cells and asthma. *Inflammation Res.* **1999**, *48*, 301–307.
(26) Brown, R. A.; Spina, D.; Page, C. P. Adenosine receptors and asthma. *Br. J. Pharmacol.* **2008**, *153*, S446–S456.
(27) Brambilla, R.; Cattabeni, F.; Ceruti, S.; Barbieri, D. *Naunyn-Schmiedeberg's Arch. Pharmacol.* **2000**, *361*, 225–234.
(28) Jacobson, K. A.; Moro, S.; Kim, Y. C.; Li, A. A_3 Adenosine receptors: protective vs damaging effects identified using novel agonists and antagonists. *Drug Dev. Res.* **1998**, *45*, 113–124.
(29) Abbracchio, M. P.; Ceruti, S.; Brambilla, R.; Barbiri, D.; Camurri, A.; Franceschi, C.; Giammaroli, A. M.; Jacobson, K. A.; Cattabeni, F.; Malorni, W. Adenosine A_3 receptors and viability of astrocytes. *Drug Dev. Res.* **1998**, *45*, 379–386.
(30) Baraldi, P. G.; Tabrizi, M. A.; Romagnoli, R.; Fruttarolo, F.; Merighi, S.; Varani, K.; Gessi, S.; Borea, P. A. Pyrazolo[4,3-e]1,2,4-triazolo[1,5-c]pyrimidine ligands, new tools to characterize A_3 adenosine receptors in human tumor cell lines. *Curr. Med. Chem.* **2005**, *12*, 1319–1329.
(31) Merighi, S.; Mirandola, P.; Varani, K.; Gessi, S.; Capitani, S.; Leung, E.; Baraldi, P. G.; Tabrizi, M. A.; Borea, P. A. Pyrazolo-triazolopyrimidine derivatives sensitize melanoma cells to the chemotherapeutic drugs: taxol and vindesine. *Biochem. Pharmacol.* **2003**, *66*, 739–748.
(32) Cosimelli, B.; Greco, G.; Ehlardo, M.; Novellino, E.; Da Settimo, F.; Taliani, S.; La Motta, C.; Bellandi, M.; Tuccinardi, T.; Martinelli, A.; Ciampi, O. Derivatives of 4-amino-6-hydroxy-2-mercaptopyrimidine as novel, potent and selective A_3 adenosine antagonists. *J. Med. Chem.* **2008**, *51*, 1764–1770.
(33) Van Veldhoven, J. P. D.; Chang, L. C. W.; von Frijtag, J. K.; Mulder-Krieger, T.; Struensee-Link, R.; Beukers, M. W.; Brussee, J.; Ijzerman, A. P. A new generation of adenosine receptor antagonists: From di- to trisubstituted aminopyrimidines. *Bioorg. Med. Chem.* **2008**, *16*, 2741–2752.
(34) Gillespie, R. J.; Bamford, S. J.; Clay, A.; Gaur, S.; Haymes, T.; Jackson, P. S.; Jordan, A. M.; Klenke, B.; Leonardi, S.; Liu, J.; Mansell, H. L.; Ng, S.; Saadi, M.; Simmonite, H.; Stratton, G. C.; Todd, R. S.; Williamson, D. S.; Yule, I. A. Antagonists of the human A_{2A} receptor. Part 6: Further optimization of pyrimidine-4-carboxamides. *Bioorg. Med. Chem.* **2009**, *17*, 6590–6605.
(35) Zhang, X.; Tellew, J. E.; Luo, Z.; Moorjani, M.; Lin, E.; Lanier, M. C.; Chen, Y.; Williams, J. P.; Saunders, J.; Lechner, S. M.; Markison, S.; Joswig, T.; Petroski, R.; Piercey, J.; Kargo, W.; Malany, S.; Santos, M.; Gross, R. S.; Wen, J.; Jalali, K.; O'Brien, Z.; Stotz, C. E.; Crespo, M. I.; Diaz, J. L.; Slee, D. H. Lead optimization of 4-acetylamino-2-(3,5-dimethylpyrazol-1-yl)-6-pyridylpyrimidines as A_{2A} adenosine receptor antagonists for the treatment of parkinson's disease. *J. Med. Chem.* **2008**, *51*, 7099–7110.
(36) Vidal, B.; Nueda, A.; Esteve, C.; Domenech, T.; Benito, S.; Reinoso, R. F.; Pont, M.; Calbet, M.; López, R.; Cadavid, M. I.; Loza, M. I.; Cárdenas, A.; Godessart, N.; Beleta, J.; Warrellow, G.; Ryder, H. Discovery and characterization of 4′-2(2-furyl)-*N*-pyridin-3-yl-4,5′-bipyrimidin-2′-amine (LAS38096), a potent, selective, and efficacious A_{2B} adenosine receptor antagonist. *J. Med. Chem.* **2007**, *50*, 2732–2736.
(37) Kuefner-Muehl, U., Scheuplein, S. W., Pohl, G., Gaida, W., Lehr, E., Mierau, J., Meade, C. J. M. Triazines with an adenosine antagonistic effect. PCT Int. Appl. WO 1999011633.
(38) Morizzo, E.; Capelli, F.; Lenzi, O.; Catarzi, D.; Varano, C.; Filachioni, G.; Vicenzi, F.; Varani, K.; Borea, P. A.; Colotta, V.; Moro, S. Scouting human A_3 adenosine receptor antagonist binding mode using a molecular simplification approach: from triazoloquinoxaline to a pyrimidine skeleton as a key study. *J. Med. Chem.* **2007**, *50*, 6596–6606.
(39) Chang, L. C. W.; Spanjersberg, R. F.; von Frijtag, J. K.; Mulder-Krieger, T.; van den Hout, G.; Beukers, M. W.; Brussee, J.; Ijzerman, A. P. 2,4,6-Trisubstituted pyrimidines as a new class of selective adenosine A_1 receptor antagonists. *J. Med. Chem.* **2004**, *47*, 6529–6540.
(40) Cheong, S. L.; Dolzhenko, A.; Kachler, S.; Paoletta, S.; Federico, S.; Cacciari, B.; Dolzhenko, A.; Koltz, K. N.; Moro, S.; Spalluto, G.; Pastorin, G. The significance of 2-furyl ring substitution with a 2-(*para*-substituted) aryl group in a new series of pyrazolo-triazolo-pyrimidines as potent and highly selective hA_3 adenosine receptors antagonists: new insights into structure−affinity relationship and receptor−antagonists recognition. *J. Med. Chem.* **2010**, *53*, 3361–3375.
(41) Priego, E. M.; Pérez-Pérez, M. J.; von Frijtag, J. K.; de Vries, H.; Ijzerman, A. P.; Camarasa, M. J.; Martín-Santamaría, S. Selective human adenosine A_3 antagonists based on pyrido[2,1-*f*]purine-2, 4-diones: novel features of hA_3 antagonist binding. *ChemMedChem* **2008**, *3*, 111–119.
(42) Baraldi, P. G.; Tabrizi, M. A.; Preti, D.; Bovero, A.; Fruttarolo, F.; Romagnoli, R.; Zaid, N. Z.; Moorman, A. R.; Varani, K.; Borea, P. A. New 2-arylpyrazolo[4,3-*c*]quinoline derivatives as potent and selective human A_3 adenosine receptor antagonists. *J. Med. Chem.* **2005**, *48*, 5001–5008.
(43) Van Muijlwijk-Kozen, J. E.; Timmerman, H.; Vollinga, R. C.; von Drabbe, J. F.; de Groote, M.; Visser, S.; Ijzerman, A. P. Thiazole and thiadiazole analogues as a novel class of adenosine receptor antagonists. *J. Med. Chem.* **2001**, *44*, 749–762.
(44) Michino, M.; Abola, E.; Brooks, C. L.; Dixon, J. S.; Moult, J.; Stevens, R. C. Community-wide assessment of GPCR structure modelling and ligand docking: GPCR Dock 2008. *Nat. Rev. Drug Discov.* **2009**, *8*, 455–463.
(45) Bondavalli, F.; Botta, M.; Bruno, O.; Ciacci, A.; Corelli, F.; Fossa, P.; Lucacchini, A.; Manetti, F.; Martini, C.; Menozzi, G.; Mosti, L.; Ranise, A.; Schenone, S.; Tafi, A.; Trincavelli, M. L. Synthesis, molecular modeling studies, and pharmacological activity of selective A_1 receptor antagonists. *J. Med. Chem.* **2002**, *45*, 4875–4887.
(46) Moro, S.; Deflorian, F.; Spalluto, G.; Pastorin, G.; Cacciari, B.; Kim, S.; Jacobson, K. A. Demystifying the three dimensional structure of G protein-coupled receptors (GPCRs) with the aid of molecular modelling. *Chem. Commun.* **2003**, *24*, 2949–2956.
(47) Jaakola, V.; Griffith, M. T.; Hanson, M. A.; Cherezov, V.; Chien, E. Y. T.; Lane, J. R.; Ijzerman, A. P.; y Stevens, R. C. The 2.6 angstrom crystal structure of a human A_{2A} adenosine receptor bound to an antagonist. *Science* **2008**, *322*, 1211–1217.
(48) Kolb, P.; Rosenbaum, D. M.; Irwin, J. J.; Fung, J. J.; Kobilka, B. K.; Shoichet, B. K. Structure-based discovery of beta 2-adrenergic receptor ligands. *Proc. Natl. Acad. Sci. U. S. A.* **2009**, *106*, 6843–6848.
(49) Lenzi, O.; Colotta, V.; Catarzi, D.; Varano, F.; Poli, D.; Filacchioni, G.; Varani, K.; Vincenzi, F.; Borea, P. A.; Paoletta, S.; Morizzo, E.; Moro, S. 2-Phenylpyrazolo[4,3-d]pyrimidin-7-one as a new scaffold to obtain potent and selective human A_3 adenosine receptor antagonists: new insights into the receptor-antagonist recognition. *J. Med. Chem.* **2009**, *52*, 7640–7652.
(50) Durán, A.; Martínez, G. C.; Pastor, M. Development and validation of AMANDA, a new algorithm for selecting highly relevant regions in Molecular Interaction Fields. *J. Chem. Inf. Model.* **2008**, *48*, 1813–1823.
(51) Duran, A. Ph.D. Thesis, University Pompeu Fabra, Barcelona, 2010. http://www.tesisenxarxa.net/TDX-0422110-094351
(52) Yaziji, V.; Coelho, A.; El Maatougui, A.; Brea, J.; Loza, M. I.; García-Mera, X.; Sotelo, E. Divergent solution-phase diarylpyrimidine libraries as selective A3 adenosine receptor antagonists. *J. Comb. Chem.* **2009**, *11*, 519–522 and references cited there.
(53) Bosch, M. P.; Campos, F.; Niubo, I.; Rosell, G.; Diaz, J. L.; Brea, J.; Loza, M. I.; Guerrero, A. Synthesis and biological activity of new potential agonists for the human adenosine A_{2A} receptor. *J. Med. Chem.* **2004**, *47*, 4041–4053.
(54) Leff, P.; Dougall, I. G. Further concerns over Cheng-Prusoff analysis. *Trends Pharmacol. Sci.* **1993**, *14*, 110–112.
(55) Verdonk, M. L.; Cole, J. C.; Hartshorn, M. J.; Murray, C. W.; Taylor, R. D. Improved protein-ligand docking using GOLD. *Proteins* **2003**, *52*, 609–623.
(56) Ballesteros, J. A.; Weinstein, H. Integrated methods for the construction of three dimensional models and computational probing of structure-function relations in G-protein coupled receptors. *Methods Neurosci.* **1995**, *25*, 366–428.
(57) Jaakola, V. P.; Lane, J. R.; Lin, J. Y.; Katritch, V; Ijzerman, A. P.; Stevens, R. C. Ligand binding and subtype selectivity of the human A_{2A} adenosine receptor: identification and characterization of essential amino acid residues. *J. Biol. Chem.* **2010**, *285*, 13032–13044.
(58) Gao, Z. G.; Chen, A.; Barak, D.; Kim, S. K.; Muller, C. E.; Jacobson, K. A. Identification by site-directed mutagenesis of residues involved in ligand recognition and activation of the

human A_3 adenosine receptor. *J. Biol. Chem.* **2002**, *277*, 19056–19063.
(59) Kim, J.; Wess, J.; van Rhee, A. M.; Schöneberg, T.; Jacobson, K. A. Mutagenesis identifies residues involved in ligand recognition in the human A_{2A} adenosine receptor. *J. Biol. Chem.* **1995**, *270*, 13987–13997.
(60) Kim, S. K.; Gao, Z. G.; Rompaey, P. V.; Gross, A. S.; Chen, A.; Calenbergh, S. V.; Jacobson, K. A. Comparison of the binding domains of A_{2A} agonists and antagonists. *J. Med. Chem.* **2003**, *46*, 4847–4859.
(61) Pastor, M.; Cruciani, G.; McLay, I.; Pickett, S.; Clementi, S. GRid-INdependent descriptors (GRIND): a novel class of alignment-independent three-dimensional molecular descriptors. *J. Med. Chem.* **2000**, *43*, 3233–3243.
(62) Tucker, A. L.; Robeva, A. S.; Taylor, H. E.; Holeton, D.; Bockner, M.; Lynch, K. R.; Linden, J. A_1 adenosine receptors. Two amino acids are responsible for species differences in ligand recognition. *J. Biol. Chem.* **1994**, *269*, 27900–27906.
(63) Ivanov, A. A.; Barak, D.; Jacobson, K. A. Evaluation of homology modeling of G-protein-coupled receptors in light of the A(2A) adenosine receptor crystallographic structure. *J. Med. Chem.* **2009**, *52*, 3284–3292.
(64) Benderitter, P.; Xavier de Araujo, J.; Schmitta, M.; Bourguignon, J. J. 2-Amino-6-iodo-4-tosyloxypyrimidine: a versatile key intermediate for regioselective functionalization of 2-aminopyrimidines in 4- and 6-positions. *Tetrahedron* **2007**, *63*, 12465–12470.
(65) Gong, B.; Hong, F.; Kohm, C.; Jenkins, S.; Tulinsky, J.; Bhatt, R.; Vries, P.; Singer, J. W.; Klein, P. Synthesis, SAR, and antitumor properties of diamino-C,Ndiarylpyrimidine positional isomers: inhibitors of lysophosphatidic acid acyltransferase-β. *Bioorg. Med. Chem. Lett.* **2004**, *14*, 2303–2308.
(66) Swarbrick, M. E.; Beswick, P. J.; Gleave, R. J.; Green, R. H.; Bingham, S.; Bountra, C.; Carter, M. C.; Chambers, L. J.; Chessell, I. P.; Clayton, N. M.; Collins, S. D.; Corfield, J. A.; Hartley, C. D.; Kleanthous, S.; Lambeth, P. F.; Lucas, F. S.; Mathews, N.; Naylor, A.; Page, L. W.; Payne, J. J.; Pegg, N. A.; Price, H. S.; Skidmore, J.; Stevens, A. J.; Stocker, R.; Stratton, S. C.; Stuart, A. J.; Wiseman, J. O. Identification of [4-[4-(methylsulfonyl)phenyl]-6-(trifluoromethyl)-2-pyrimidinyl] amines and ethers as potent and selective cyclooxygenase-2 inhibitors. *Bioorg. Med. Chem. Lett.* **2009**, *19*, 4504–4508.
(67) Thompson, J. D.; Higgins, D. G.; Gibson, T. J. CLUSTAL W: improving the sensitivity of progressive multiple sequence alignment through sequence weighting, position-specific gap penalties and weight matrix choice. *Nucleic Acid Res.* **1994**, *22*, 4673–4680.
(68) Sali, A.; Blundell, T. L. Comparative protein modelling by satisfaction of spatial restraints. *J. Mol. Biol.* **1993**, *234*, 779–815.
(69) Laskowski, R. A.; MacArthur, M. W.; Moss, D. S.; y Thornton, J. M. PROCHECK: a program to check the stereochemical quality of protein structures. *J. Appl. Crystallogr.* **1993**, *26*, 283–291.
(70) Davis, I. W.; Leaver-Fay, A.; Chen, V. B.; Block, J. N.; Kapral, G. J.; Wang, X.; Murray, L. W.; Arendall, W. B.; Snoeyink, J.; Richardson, J. S.; Richardson, D. C. MolProbity: all-atom contacts and structure validation for proteins and nucleic acids. *Nucleic Acids Res.* **2007**, *35*, W375–383.
(71) Fiser, A.; Do, R. K.; Sali, A. Modeling of loops in protein structures. *Protein Sci.* **2000**, *9*, 1753–1773.
(72) *Macromodel*, version 9.7; Schrödinger, LLC: New York, NY, 2009.
(73) Jones, G.; Willett, P.; Glen, R. C.; Leach, A. R.; Taylor, R. Development and validation of a genetic algorithm for flexible docking. *J. Mol. Biol.* **1997**, *267*, 727–748.
(74) *MOE* (*Molecular Operative Environment*), version 2009.10; Chemical Computing Group Inc. Montreal, Canada; 2009.
(75) *Pentacle*, version 1.1; Molecular Discovery, Ltd.: Perugia, Italy, 2009.
(76) Goodford, P. J. A computational procedure for determining energetically favorable binding sites of biological important macromolecules. *J. Med. Chem.* **1985**, *28*, 849–857.